Title
Exploiting natural dynamics for gait generation in undulatory locomotion

Journal
International Journal of Control, 93(2)

ISSN
0020-7179

Authors
Ludeke, Taylor
Iwasaki, Tetsuya

Publication Date
2020-02-01

DOI
10.1080/00207179.2019.1569763

Peer reviewed

Exploiting Natural Dynamics for Gait Generation in Undulatory Locomotion

Taylor Ludeke and Tetsuya Iwasaki

UCLA Mechanical & Aerospace Engineering, Los Angeles, CA 90095, USA

ARTICLE HISTORY
Compiled March 10, 2018

ABSTRACT
Robotic vehicles inspired by animal locomotion are propelled by interactive forces from the environment resulting from periodic body movements. The pattern of body oscillation (gait) can be mimicked from animals, but understanding the principles underlying the gait generation would allow for flexible and broad applications to match and go beyond the performance of the nature's design. We hypothesize that the traveling-wave oscillations, often observed in undulatory locomotion, can be characterized as a natural oscillation of the locomotion dynamics, and propose a formal definition of the natural gait for locomotion systems. We first identify the dynamics essential to undulatory locomotion, and define the mode shape of natural oscillation by the free response of an idealized system. We then use body-environment resonance to define the amplitude and frequency of the oscillations. Explicit formulas for the natural gait are derived to provide insight into the mechanisms underlying undulatory locomotion. An example of leech swimming illustrates how undulatory gaits similar to those observed can be produced as the natural gait, and how they can be modulated to achieve a variety of swim speeds.

KEYWORDS
Oscillation; Locomotion; Resonance; Natural mode

1. Introduction

Animal locomotion has been studied for decades by engineers and scientists with overlapping objectives. Scientific study of animal locomotion has contributed to a better understanding of biological mechanisms underlying various functionalities such as adaptability, efficiency, and agility. The knowledge thus generated is useful for developing biologically inspired robots (Ijspeert, 2014; Sitti, Menciassi, Ijspeert, Low, & Kim, 2013). Development of robotic locomotors involves selection of gaits (periodic body movements leading to sustained traveling velocity) in addition to mechanical design of body, actuation, sensing, and control. In most designs, both body shape and gait are designed by mimicking animals. For example, observed undulatory movements of snakes or fish are parametrized and used to set the basic motion primitives and possibly optimize a cost function in robotic locomotors (Curet, Patankar, Lauder, & MacIver, 2011; Hatton & Choset, 2010; Saito, Fukaya, & Iwasaki, 2002; Tesch et al., 2009). This type of biomimicry has also been used for legged locomotion (Fukuoka, Kimura, & Cohen, 2003; Grizzle, Abba, & Plestan, 2001) as well as for gait transition

CONTACT Tetsuya Iwasaki. Email: tiwasaki@ucla.edu

from swimming to walking (Ijspeert, Crespi, Ryczko, & Cabelguen, 2007). While these results produced effective robotic locomotors with some success, deeper understanding of biology and systematic theories for gait determination would enable the generation of adaptable gaits and possibly non-intuitive gaits that could go beyond mimicking animals in achieving desired properties.

A common approach to gait selection is to search for an optimal gait. Optimization is useful because it is based on contrived metrics which can be clearly defined for mathematical analysis. Existing strategies include quadratic optimization over all periodic motions (Blair & Iwasaki, 2011; Kohannim & Iwasaki, 2017), parametrization of the geometric configuration over a truncated basis (Cortes, Martinez, Ostrowski, & McIsaac, 2001), calculus of variations (Hicks & Ito, 2005), and mimicking observed kinematics to reduce the number of parameters which are then optimized numerically by gridding the parameter space (McIsaac & Ostrowski, 2003). Some of these methods have been successfully applied to reproduce biological gaits with no presumption on the kinematics (Liu, Fish, Russo, Blemker, & Iwasaki, 2016). However, these optimization methods are based on numerical computations, and hence the results are not as transparent or insightful as analytical closed-form solutions, and may not explain why a particular gait makes sense physically.

An alternative approach to gait design may be through natural oscillations or resonance. There is evidence that animals exploit resonance during locomotion (Ahlborn, Blake, & Megill, 2006). Experiments have shown that a natural walking stride conforms to the resonant frequency of the limbs when they are modeled as pendulums (Holt, Hamill, & Anders, 1991; Wagenaar & van Emmerik, 2000). Mathematical analysis of inertial swimmers (high Reynolds number swimming) supports the existence of resonance peaks when considering muscle tension (Kohannim & Iwasaki, 2014), travel speed, and efficiency (Gazzola, Argentina, & Mahadevan, 2015) with respect to frequency. Animals can also tune the resonance frequency of their bodies. Limbed animals can redistribute mass by bending their limbs, changing the resonance frequency when they switch between walking and running gaits (Ahlborn et al., 2006). Fish can activate the muscles on both sides of their body to alter their body stiffness (Long & Jr., 1998). Thus, resonance mechanisms underlying animal locomotion may suggest ways to design gaits for robotic systems.

Resonance phenomena in animal locomotion has been extensively studied through fluid mechanics of swimming and flying. Wake resonance is defined for the motion of the fluid surrounding the oscillating body (e.g. fin), and has been studied experimentally using particle image velocimetry or computationally through simulation and analysis based on the Navier Stokes equations (Moored, Dewey, Smits, & Haj-Hariri, 2012; Triantafyllou, Triantafyllou, & Yue, 2000). In the study of hydrodynamic resonance, the body movements are typically prescribed, either by mimicking observed kinematics (Borazjani & Sotiropoulos, 2008, 2009) or parameterizing the motion by frequency and amplitude (Lewin & Haj-Hariri, 2003). Hence, the resonance is exclusively due to the fluid motion and is independent of body flexibility. The effect of body flexibility on anguilliform swimming has been examined and flapping tail resonance is found to contribute to increasing propulsive force (Leftwich, Tytell, Cohen, & Smits, 2012). However, it remains obscure how the resonances of body and fluid interact with each other to determine the overall gait.

A way to avoid prescribed kinematics and define the overall gait is passive locomotion resulting from the inherent natural dynamics. The overall gait is defined by a periodic body movement sustained as a "natural oscillation" (or free response) of the body-environment dynamics. The gait has an intrinsic frequency and a correspond-

ing mode shape which describes the pattern of oscillation for the multiple degrees of freedom. For instance, bipedal robots on a slope, with limbs that are allowed to swing freely within morphological constraints, were found to have gaits similar to observed human walking (McGeer, 1990). For such passive walkers, the environment (i.e. gravity field) provides a power source, and the gait is essentially determined by the body properties (Collins, Ruina, Tedrake, & Wissei, 2005; Ijspeert, 2008). For non-pedal locomotion such as swimming and crawling, however, body undulation has not been characterized as a free response of autonomous dynamics.

In this paper, we will present a mathematical characterization for undulatory gaits based on natural modes of oscillation and body-environment resonance. To the authors' knowledge, there has been no rigorous model-based analysis of the traveling body wave observed in the undulatory gait of slender-body animals. Nor has a comprehensive definition for resonance, incorporating the body and the environment, been established for undulatory locomotion. We seek the origin of traveling waves within natural oscillations without prescribing such motion. We also develop analytical insights into the frequency and amplitude of undulation in terms of resonance resulting from dynamic interactions of the body and environment.

First, we present simple mathematical models for undulatory locomotion that capture the essential dynamics of body and environment. We consider the long, slender body with no limbs or other appendages. This body type, which epitomizes a user of the undulatory gait, can be modeled with good accuracy as a chain of rigid links connected by flexible joints. Additionally we consider the environmental forces acting on the body to be resistive, meaning the forces correlate positively with the relative velocities between the body and environment. Simple models are developed from laws of physics with approximations under small amplitude oscillations and averaging over an undulation cycle.

We then use the models to give precise definitions of natural oscillation and resonance for the body-environment system so that the resulting motion resembles the undulatory gaits observed in nature. Resonance and natural modes of oscillation have well established definitions for "standard" linear mechanical systems described by mass, stiffness, and damping matrices that are symmetric positive (semi)definite. The natural modes of oscillation are defined as the periodic solutions of the idealized system where the damping is removed. For undulatory locomotion, however, the traditional definition does not apply since nonlinearities in the system and resistive (damping) forces are essential for thrust generation (Blair & Iwasaki, 2011), and lead to an asymmetric stiffness matrix (Z. Chen, Iwasaki, & Zhu, 2015).

Nevertheless, we hypothesize that the traditional concepts can be extended to explain the body oscillations that occur in undulatory locomotion, in spite of the dynamics being more complex and dependent on resistive forces. In particular, we provide an analogous definition for natural modes of oscillation as the free response to an idealized system in which body mass, body stiffness, and purely dissipative drag forces are removed. This explains the traveling waves. Fixing the mode shape in this way, we seek body-environment resonance, at which the frequency and amplitude maximize the gain from the input bending moment to the travel velocity. This combination of natural modes of oscillation and body-environment resonance forms our definition for a natural gait, which is fully characterized in terms of analytical, closed form expressions. Our result provides a unique approach to both gait selection and the ongoing attempt to understand what makes an observed gait natural.

Some preliminary results were reported in (Ludeke & Iwasaki, 2017) without proofs. This paper expands on those results with more in depth analysis and complete proofs. The case study of leech swimming provided here is new.

2. The Dynamics of Undulatory Locomotion

Undulatory gaits are typically used by animals with long, thin bodies, such as eels and snakes. Such locomotion depends on directional anisotropy in the interactive force between the body and its environment (i.e. larger normal force than tangential force) to rectify local periodic joint movement into global linear motion (Blair & Iwasaki, 2011; Hirose, 1993; Saito et al., 2002). To model the dynamics of undulatory locomotion, we represent the robotic or animal body as a chain of n rigid links connected by $n-1$ flexible joints as shown in Fig. 1. Only planar motion is considered. The direction of travel is considered to be along the x-axis.

Each joint is assigned a linear spring stiffness to account for the elasticity of the body. Bending moment $u \in \mathbb{R}^{n-1}$ is applied by actuators/muscles at the joints. The interactive force from the environment is assumed proportional to the relative velocity with a larger drag/friction coefficient in the normal direction than that in the tangential direction. Examples of locomotion that depends on these type of resistive forces are low Reynolds number swimming and snake crawling. The reactive hydrodynamic force (or added-mass effect), which is known to be dominant in fish swimming with a caudal fin (Lighthill, 1969), is not important in undulatory swimming (J. Chen, Friesen, & Iwasaki, 2011) and therefore not considered here. The model is crude, but captures the most essential dynamics for thrust generation in undulatory locomotion.

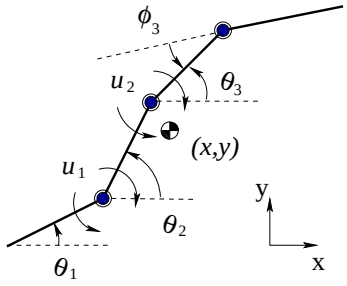

Figure 1. The link-chain model for undulator (case $n = 4$).

The equations of motion are developed by balancing the moments and forces acting on the links in a manner similar to that used in (Blair & Iwasaki, 2011; Saito et al., 2002). Let $\theta \in \mathbb{R}^n$ be the link angles as in Fig. 1, and $(v_x, v_y) := (\dot{x}, \dot{y}) \in \mathbb{R}^2$ be the locomotion velocity of the mass center of the whole body. Assuming that the body deformation θ and the velocity component v_y orthogonal to the direction of locomotion are small and of order ε, the fully nonlinear equations of motion are simplified by neglecting the $O(\varepsilon^3)$ terms as follows:

$$\begin{bmatrix} J\ddot{\theta} + K\theta - Bu \\ m\dot{v}_x \\ m\dot{v}_y \end{bmatrix} + \begin{bmatrix} D & \Lambda\theta & -F^\mathsf{T} C_n e \\ \theta^\mathsf{T}\Lambda^\mathsf{T} & e^\mathsf{T} C_t e + \theta^\mathsf{T} C_o \theta & -\theta^\mathsf{T} C_o e \\ -e^\mathsf{T} C_n F & -e^\mathsf{T} C_o \theta & e^\mathsf{T} C_n e \end{bmatrix} \begin{bmatrix} \dot{\theta} \\ v_x \\ v_y \end{bmatrix} = 0, \qquad (1)$$

where the coefficient matrices, as well as all other matrices to be used in this paper,

are defined in Appendix A. The first term captures the inertial forces, body stiffness, and bending moment, while the second term captures the forces from the environment. Assuming that the body is modeled by uniform links, we have

$$M = m_o I, \quad L = \ell_o I, \quad C_n = c_n I, \quad C_t = c_t I, \quad K = kBB^{\mathsf{T}}, \tag{2}$$

where m_o and $2\ell_o$ are the mass and length of each link, k is the bending stiffness of each joint, and c_n and c_t are the normal and tangential drag/friction coefficients for the linear environmental force acting on each link. We will impose the uniform link assumption on the model throughout the paper.

The link angle vector $\theta \in \mathbb{R}^n$ contains information on the body shape $\phi \in \mathbb{R}^{n-1}$ and orientation $\theta_o \in \mathbb{R}$, where $\phi_i := \theta_i - \theta_{i+1}$ are the joint angles and θ_o is defined to be the average of link angles θ_i. In particular, they are related by the coordinate transformation $\theta \leftrightarrow (\phi, \theta_o)$ defined by

$$\begin{bmatrix} \phi \\ \theta_o \end{bmatrix} = \begin{bmatrix} B^{\mathsf{T}} \\ e^{\mathsf{T}}/n \end{bmatrix} \theta \quad \text{or} \quad \theta = T\phi + e\theta_o, \tag{3}$$

where $T := B(B^{\mathsf{T}}B)^{-1}$ is the Moore-Penrose inverse of B^{T}. A gait is a periodic function $\phi(t)$ describing a rhythmic body motion. A proper gait for locomotion is generated by periodic joint torques $u(t)$, and results in periodic velocity (v_x, v_y) and orientation θ_o, where the average value of v_x is nonzero and those for v_y and θ_o are zero.

For analytical study of gaits, we will further simplify the model by introducing fictitious forces f_x and f_y and toque τ uniformly acting on all the links to remove oscillations in v_x, v_y, and θ_o, respectively. These additional forces will replace the zero vector on the right hand side of (1) by column vector $(e\tau, f_x, f_y)$, which is periodic with zero average because its role is only to remove the ripples and the main thrust for locomotion should come from the environmental force resulting from a periodic body motion. The following two lemmas provide models with two levels of reduced complexity.

Lemma 2.1. *Consider the model (1) with additional input vector $(e\tau, f_x, f_y)$ on the right hand side. Suppose $\tau \equiv 0$ and (f_x, f_y) are $\mathcal{T}$-periodic with zero average and keep the locomotion velocity constant at $(v_x, v_y) \equiv (v_o, 0)$. Then $\mathcal{T}$-periodic signals (u, θ) satisfy the augmented model equation if and only if*

$$\begin{aligned} &J\ddot{\theta} + D\dot{\theta} + (K + v_o\Lambda)\theta = Bu \\ &\int_0^{\mathcal{T}} \Big(\dot{\theta}^{\mathsf{T}}\Lambda\theta + (e^{\mathsf{T}}C_t e + \theta^{\mathsf{T}}C_o\theta)v_o\Big)dt = 0 \\ &\int_0^{\mathcal{T}} \theta_o\, dt = 0 \end{aligned} \tag{4}$$

Proof. When the fictitious forces (f_x, f_y) remove the influence of oscillations in the velocity such that $(v_x, v_y) \equiv (v_o, 0)$, the first equation in (4) is equivalent to the first line in (1). The other equations in (4) are obtained by integrating the second and third lines in (1) over one period and noting that the average of (f_x, f_y) is zero. Examination of the definitions in Appendix A shows that $e^{\mathsf{T}}C_nF = 0$ under the uniformity assumption. □

Lemma 2.2. *Consider the model (1) with additional input vector $(e\tau, f_x, f_y)$ on the right hand side. Suppose $f_y \equiv 0$ and (τ, f_x) are $\mathcal{T}$-periodic with zero average and keep the locomotion speed and orientation constant at $(v_x, \theta_o) \equiv (v_o, 0)$. Then $\mathcal{T}$-periodic signals (u, ϕ, v_y) satisfy the augmented model equation if and only if*

$$\begin{aligned} &\mathsf{J}\ddot{\phi} + \mathsf{D}\dot{\phi} + (\mathcal{K} + v_o\Lambda)\phi = u \\ &\int_0^{\mathcal{T}} \Big(\dot{\phi}^{\mathsf{T}}\Lambda\phi + (e^{\mathsf{T}}C_t e + \phi^{\mathsf{T}}\mathsf{C}_o\phi)v_o\Big)dt = 0 \\ &\int_0^{\mathcal{T}} e^{\mathsf{T}}\Lambda T\phi\, dt = 0, \quad v_y \equiv 0 \end{aligned} \tag{5}$$

where, with T in (3),

$$\mathsf{J} := T^{\mathsf{T}}JT, \quad \mathsf{D} := T^{\mathsf{T}}DT, \quad \Lambda := T^{\mathsf{T}}\Lambda T, \quad \mathsf{C}_o := T^{\mathsf{T}}C_oT.$$

Proof. Given signals (u, ϕ, v_y), together with $(v_x, \theta_o) \equiv (v_o, 0)$, satisfy (1) with the fictitious inputs if and only if

$$\begin{bmatrix} \mathsf{J}\ddot{\phi} + \mathsf{D}\dot{\phi} + (v_o\Lambda + \mathcal{K})\phi - u \\ e^{\mathsf{T}}JT\ddot{\phi} + e^{\mathsf{T}}DT\dot{\phi} + v_o e^{\mathsf{T}}\Lambda T\phi \\ \phi^{\mathsf{T}}\Lambda^{\mathsf{T}}\dot{\phi} + v_o(e^{\mathsf{T}}C_t e + \phi^{\mathsf{T}}\mathsf{C}_o\phi) \\ m\dot{v}_y + e^{\mathsf{T}}C_n e\, v_y \end{bmatrix} = \begin{bmatrix} 0 \\ e^{\mathsf{T}}e\tau \\ f_x \\ 0 \end{bmatrix},$$

where the transformation in (3) is applied, and we noted $T^{\mathsf{T}}B$, $e^{\mathsf{T}}B$, and $T^{\mathsf{T}}e$ are all zero by definition. Thus the first row gives the fist equation in (5). Averaging the second and third rows over one period $\mathcal{T}$ gives the two integral equations in (5), recalling that (τ, f_x) averages zero over one period. Finally, periodic v_y satisfying the fourth row is uniquely determined as $v_y \equiv 0$. □

3. Natural Gait

We seek a gait $\phi(t)$ that is characterized in terms of a natural oscillation and resonance of the models developed in the previous section. In particular, we define a unique gait such that the oscillation pattern (relative timing and amplitude of the joint oscillations) is specified as a mode shape of natural oscillation for idealized dynamics, while the frequency and amplitude are determined by resonance in the coupled body-environment system. We will refer to this as the natural gait since it exploits natural dynamics to achieve efficient locomotion.

3.1. Natural Oscillation

We consider natural oscillation to be a periodic solution to the free response equation of a system that has been idealized to sustain oscillation without external forcing. Removal of damping is the process for such idealization for standard mechanical systems (e.g. a pendulum subject to friction). For locomotion systems, the drag from the environment gives damping terms, but cannot be removed completely since thrust for locomotion is generated from part of this force. This section will show a proper

idealization wherein the modified dynamics admit a periodic solution appropriate for undulatory locomotion and characterize natural oscillations.

The origin of traveling waves observed in undulatory locomotion may reside in the dynamics of body-environment interactions. Based on this idea, we define the idealized system by neglecting body mass, body stiffness, and the portion of the environmental drag that cannot contribute to thrust generation. Clearly, the drag force tangent to each link always resists forward locomotion and can be removed by setting $C_t = 0$. The drag force normal to each link can have both positive and negative contributions to thrust generation. It turns out that the negative portion is exactly captured by the torsional drag $D_\tau \dot{\phi}$, which is due to pure rotation about the center of mass for a given link and results only in energy loss as does tangential drag.

Theorem 3.1. *Consider the model in (1). Suppose the body has no inertia ($J = 0$), no stiffness ($K = 0$), and no active bending moment ($u(t) \equiv 0$). Further assume that there is no tangential drag ($C_t = 0$) or torsional drag ($D_\tau = 0$). Then the motion variables $(\phi, \theta_o, v_x, v_y)$ satisfy the model equation if and only if*

$$\Delta\dot{\phi} + v_x\phi + \delta\dot{\theta}_o = 0, \quad v_x\theta_o = v_y, \quad \Delta := ALT, \quad \delta := ALe. \tag{6}$$

In particular, for a constant $v_o \in \mathbb{R}$, the gait specified by

$$\phi(t) = \Re[\hat{\phi}e^{j\omega t}], \quad (j\omega\Delta + v_o I)\hat{\phi} = 0 \tag{7}$$

satisfies the dynamics in (6) with associated velocities and orientation $(v_x, v_y, \theta_o) \equiv (v_o, 0, 0)$, where $\hat{\phi} \in \mathbb{C}^{n-1}$ and $\omega \in \mathbb{R}$ are a nonzero vector and scalar.

Proof. The model in (1) under the idealized condition reduces to

$$\begin{bmatrix} F^\mathsf{T}C_nF & F^\mathsf{T}C_n\theta & -F^\mathsf{T}C_ne \\ \theta^\mathsf{T}C_nF & \theta^\mathsf{T}C_n & -\theta^\mathsf{T}C_ne \\ -e^\mathsf{T}C_nF & -e^\mathsf{T}C_n\theta & e^\mathsf{T}C_ne \end{bmatrix} \begin{bmatrix} \dot{\theta} \\ v_x \\ v_y \end{bmatrix} = 0, \tag{8}$$

which, through factorization of the coefficient matrix, is equivalent to

$$F\dot{\theta} + v_x\theta - v_ye = 0.$$

Then using the coordinate transformation in (3) and the definition of F in Appendix A, this equation is equivalent to

$$\begin{bmatrix} ALT & ALe \\ 0 & 0 \end{bmatrix} \begin{bmatrix} \dot{\phi} \\ \dot{\theta}_o \end{bmatrix} + \begin{bmatrix} \phi \\ \theta_o \end{bmatrix} v_x - \begin{bmatrix} 0 \\ 1 \end{bmatrix} v_y = 0.$$

Thus we have the system in (6). All the eigenvalues of Δ are purely imaginary because of the similarity

$$U\Delta U^{-1} = \ell_o UABU, \quad U := (B^\mathsf{T}B)^{-1/2},$$

where AB is skew symmetric and U is symmetric. Thus the harmonic gait specified in (7) is well defined, and can readily been shown to satisfy the equations of motion in (6). □

For each locomotion speed v_o, the natural oscillations of (1) are now characterized by (7), which are periodic solutions of the idealized dynamics (8). It turned out that the natural oscillation is harmonic:

$$\phi_i(t) = \alpha_i \cos(\omega t + \beta_i), \quad \alpha_i e^{j\beta_i} := \hat{\phi}_i, \quad i = 1, 2, \ldots, n-1.$$

All $n-1$ eigenvalues of Δ are distinct and lie on the imaginary axis, one of which is at the origin if n is even. For each nonzero eigenvalue λ of Δ, the mode shape $\hat{\phi}$ is uniquely determined (up to a scalar multiple) as the corresponding eigenvector, while the natural frequency ω linearly varies with the locomotion speed v_o as $\omega = jv_o/\lambda$. It can be verified that eigenvalues $\lambda = jp_{\mathfrak{m}}$ with $p_{\mathfrak{m}} > 0$ and corresponding eigenvectors $z_{\mathfrak{m}}$ of Δ are given by

$$p_{\mathfrak{m}} = \frac{\ell_o}{\tan\theta_{\mathfrak{m}}}, \quad z_{\mathfrak{m}i} = \frac{e^{j(2i\theta_{\mathfrak{m}})}}{\sqrt{n-1}}, \quad \theta_{\mathfrak{m}} := \frac{\mathfrak{m}\pi}{n}, \tag{9}$$

for $\mathfrak{m} = 1, \ldots, \lfloor (n-1)/2 \rfloor$, where $z_{\mathfrak{m}i} \in \mathbb{C}$ is the i^{th} entry of the $\mathfrak{m}^{\text{th}}$ eigenvector $z_{\mathfrak{m}} \in \mathbb{C}^{n-1}$ which is normalized such that $\|z_{\mathfrak{m}}\| = 1$. Note in particular that, for each $\mathfrak{m}$, the magnitudes $z_{\mathfrak{m}i}$ are uniform over i, which means that the oscillation amplitudes are uniform for all joint angles $\phi_i(t)$ along the body. Moreover, the phase angles of $z_{\mathfrak{m}i}$ are equally spaced over $2\mathfrak{m}\pi$, which translates to traveling waves exhibited by the body with the number of waves equal to $\mathfrak{m}$. For a given locomotion speed v_o, the natural frequency ω is the smallest for the 1st mode.

The body shape described by $\phi(t)$ in (7) is depicted in Fig. 2 at six evenly spaced time instances during one cycle for two modes of natural oscillations, where the number of links is $n = 18$ and $\hat{\phi} = \gamma z_{\mathfrak{m}}$ with $\mathfrak{m} = 1, 2$ and $\gamma = 0.914, 1.828$Rad. Each oscillation exhibits body waves traveling to the left as indicated by the diagonal lines marking the path of the apex of the body wave. The waves push the environment (e.g. ground for crawling and water for swimming), creating thrust to move the body to the right. The amplitude of body undulation depends on the magnitude of $\|\hat{\phi}\|$, which is unspecified in (7) and is chosen arbitrarily in the snapshots in Fig. 2 .

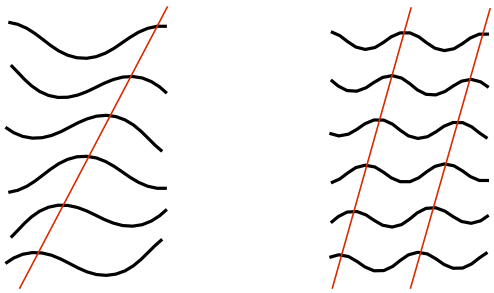

Figure 2. Oscillation patterns for 1st and 2nd modes of natural oscillation.

The natural oscillation in (7) by itself is not adequate for defining a reasonable gait because it has an undefined amplitude and may not result in locomotion speed $v_x = v_o$ when subject to the full dynamics in the system in (1). To define the natural gait (as opposed to the natural oscillation) consistently with the original models, we adopt the mode shape as only one of its defining properties.

Definition 3.2. The mode shape, $z \in \mathbb{C}^{n-1}$, of a natural gait is defined by the eigenvector of Δ in (6), associated with a nonzero eigenvalue (denoted by jp):

$$\Delta z = jpz, \quad p \neq 0, \quad \|z\| = 1. \tag{10}$$

where the magnitude is normalized.

The natural gait is of the form $\phi(t) = \Re[\gamma z e^{j\omega t}]$ where z is the mode shape specified in Definition 3.2. We will specify the amplitude γ and frequency ω based on resonance.

3.2. Resonance

Suppose the body undulates with harmonic gait $\phi(t) = \Re[\gamma z e^{j\omega t}]$ with period $\mathcal{T} := 2\pi/\omega$, where z is the mode shape as specified in Definition 3.2, and γ and ω are arbitrary constants. Let $u(t)$ be the $\mathcal{T}$-periodic bending moment input that generates this gait, and v_o be the resulting locomotion velocity, in accordance with (4) or (5). Consider the gain from bending moment to locomotion speed:

$$G(\omega, \gamma) := \frac{v_o}{u_{\mathrm{RMS}}}, \quad u_{\mathrm{RMS}} := \sqrt{\frac{1}{\mathcal{T}} \int_0^{\mathcal{T}} \|u(t)\|^2 dt}, \tag{11}$$

which dictates effectiveness of the gait; larger G means that faster locomotion is achieved with smaller actuation effort. When G takes the maximum value over a range of (ω, γ), we say that the gait achieves resonance. We use this property to define the natural gait.

Definition 3.3. The frequency ω and amplitude γ of the natural gait $\phi(t) = \Re[\gamma z e^{j\omega t}]$ are those achieving resonance in the body-environment dynamics to maximize the gain in (11) subject to (4) or (5), where the mode shape z is specified in Definition 3.2.

The following result is useful for determining the resonant frequency and amplitude.

Lemma 3.4. *Consider the model in (4) with an arbitrary gait of the form* $\phi(t) = \Re[\gamma z e^{j\omega t}]$. *The gain in (11) with* $\mathcal{T} := 2\pi/\omega$ *can be calculated as*

$$G(\omega, \gamma) = \frac{\sqrt{2}\, v_o}{\|\hat{u}\|}, \tag{12}$$

$$\hat{u} := (\mathcal{K} + v_o \mathcal{L} - \mathcal{J}\omega^2 + j\omega \mathcal{D})\hat{\phi}, \quad \hat{\phi} = \gamma z. \tag{13}$$

where v_o *is a real root of the 3rd order polynomial given by*

$$\begin{aligned} &\big(2e^{\mathsf{T}} C_t e + \hat{\theta}^* C_o \hat{\theta}\big) v_o = j\omega \hat{\theta}^* S \hat{\theta}, \\ &\hat{\theta} := (X + v_o Y)\hat{\phi}, \quad S := (\Lambda - \Lambda^{\mathsf{T}})/2, \\ &X := T - eh^{\mathsf{T}}, \quad Y := e\Lambda_{21}/(\omega^2 J_{22} - j\omega D_{22}) \end{aligned} \tag{14}$$

and the coefficient matrices are defined in Appendix A.

Proof. With (ϕ, θ_o) in (3), let us introduce another variable $\varphi := \theta_o + h^{\mathsf{T}}\phi$ where h is defined in (A2) in Appendix A. Through the coordinate transformation $\theta \leftrightarrow (\phi, \varphi)$,

the first equation in (4) is equivalent to

$$\begin{aligned} \mathcal{J}\ddot{\phi} + \mathcal{D}\dot{\phi} + v_o\mathcal{L}\phi + \mathcal{K}\phi &= u, \\ J_{22}\ddot{\varphi} + D_{22}\dot{\varphi} + v_o\Lambda_{21}\phi &= 0, \end{aligned} \tag{15}$$

where the terms are defined by (A2) in Appendix A. Therefore, the bending moment $u(t)$ that generates a given gait $\phi(t) = \Re[\hat{\phi}e^{j\omega t}]$ in accordance with the first equation in (4) can be uniquely determined as $u(t) = \Re[\hat{u}e^{j\omega t}]$ with $\hat{u}$ in (13). For this $u(t)$ the average of magnitude $\|u(t)\|^2$ over one period as specified in (11) is given by $\|\hat{u}\|^2/2$. Solving the second equation in (15) for steady state $\varphi(t)$, we have

$$\varphi(t) = \Re[\hat{\varphi}e^{j\omega t}], \quad \hat{\varphi} := (v_o\Lambda_{21}\hat{\phi})/(\omega^2 J_{22} - j\omega D_{22}).$$

The original variable $\theta(t)$ can then be obtained by the transformation $\theta \leftrightarrow (\phi, \varphi)$ as

$$\theta(t) = \Re[\hat{\theta}e^{j\omega t}], \quad \hat{\theta} = (T - eh^{\mathsf{T}})\hat{\phi} + e\hat{\varphi} = (X + v_oY)\hat{\phi}.$$

Since $\theta(t)$ is unbiased, so is $\theta_o := e^{\mathsf{T}}\theta/n$ and the third condition in (4) is satisfied. Finally, the velocity v_o resulting from the gait $\phi(t)$ is determined by the phasor form of the second equation in (4), as given in (14). □

The 3rd order polynomial in (14) may have multiple real solutions for v_o in general. However, uniqueness is expected because one gait, with all other parameters fixed, cannot result in multiple constant, steady-state velocities. This presumption is supported by our numerical investigations which always resulted in one real and two imaginary solutions for v_o. With the gain G determined for each pair (ω, γ), the resonant frequency and amplitude that maximize G can be computed by gridding the (ω, γ) plane. The method works for an arbitrary oscillation pattern $z \in \mathbb{C}^{n-1}$ which is not necessarily a mode shape for natural oscillation.

4. Analytical Study of Resonance

The equations for calculating the gain G for the model in (4) as specified in Lemma 3.4 do not allow a closed form characterization of resonance. Explicit formulas for the resonant frequency and amplitude can, however, be derived for the model in (5) which further simplifies (4) by $\theta_o \equiv 0$. The pitching oscillation of the body orientation denoted by $\theta_o(t)$ is fairly small in amplitude during undulatory locomotion whether observed in nature or described by the model in (4) for a given input $u(t)$. Therefore, we use (5) for analysis in this section to gain insights into mechanisms underlying the body-environment resonance.

4.1. Formulas for Resonance Frequency and Amplitude

The following result provides explicit, closed-form formulas for characterizing the resonance.

Theorem 4.1. *Let a gait $\phi(t) = \Re[\gamma z e^{j\omega t}]$ be given with z in Definition 3.2 and consider the model in (5). The gain in (11) takes the maximum over all (ω, γ) satisfying*

(5) when

$$\begin{aligned}\omega &= \sqrt{\frac{\|\mathcal{K}z\|}{\|\mathrm{J}z\|}}, \quad v_o = \frac{\gamma^2 z^*(j\omega\Lambda)z}{\gamma^2 z^*\mathrm{C}_o z + 2e^\mathsf{T}C_t e},\\ \gamma &= \sqrt[4]{\frac{(2e^\mathsf{T}C_t e)^2(\|(\mathrm{J}\omega^2-\mathcal{K})z\|^2 + \|\omega\mathrm{D}z\|^2)}{(z^*\mathrm{C}_o z)^2\|(\mathrm{J}\omega^2-\mathcal{K})z\|^2 + (z^*Pz)^2\|\omega\mathrm{D}z\|^2}}\end{aligned} \tag{16}$$

where, using p in Definition 3.2,

$$P := j\sigma\Lambda - \mathrm{C}_o, \quad \sigma := \frac{p}{p^2+\ell_o^2/3}\Big(1-\frac{c_t}{c_n}\Big). \tag{17}$$

Proof. The gait $\phi(t)$ is unbiased and hence satisfies the integral equation in the third line of (5). From the first equation in (5), the input $u(t)$ that results in the gait $\phi(t)$ is given by

$$\begin{aligned}&u(t) = \Re[\hat{u}e^{j\omega t}], \quad \hat{u} = Q(j\omega)\hat{\phi}, \quad \hat{\phi} := \gamma z,\\ &Q(s) := s^2\mathrm{J} + s\mathrm{D} + v_o\Lambda + \mathcal{K}.\end{aligned} \tag{18}$$

The second equation in (5) holds if and only if

$$\Big(2e^\mathsf{T}C_t e + \hat{\phi}^*\mathrm{C}_o\hat{\phi}\Big)v_o = j\omega\hat{\phi}^*\Lambda\hat{\phi}, \tag{19}$$

where by definition, Λ is skew symmetric under assumption (2) so the right hand side is a real number. The gain in (11) is now given by (12) with $\hat{u}$ in (18) and v_o in (16) obtained by solving the *linear* equation (19).

First consider the ω that maximizes G for a fixed γ. From (19) it is clear that the ratio v_o/ω is fixed by γ. Substituting $\hat{u}$ from (18) into (12) and rearranging terms gives

$$G = \frac{\sqrt{2}\,v_o/\omega}{\gamma\|\mathrm{Q}(j\omega)z\|}, \quad \mathrm{Q}(s) := Q(s)/\omega.$$

Recalling that (jp, z) is an eigenvalue-eigenvector pair of Δ as specified in Definition 3.2, it can be verified that

$$\begin{aligned}&\mathrm{J}z = m_o\mathfrak{p}y, && j\Lambda z = c_o p y,\\ &\mathrm{D}z = c_n\mathfrak{p}y, && z^*\mathrm{C}_o z = c_o\|By\|^2,\\ &y := (B^\mathsf{T}B)^{-1}z, && \mathfrak{p} := p^2+\ell_o^2/3, \quad c_o := c_n - c_t\end{aligned} \tag{20}$$

hold. Noting in particular that $j\Lambda z = \sigma\mathrm{D}z$, we have

$$\mathrm{Q}(j\omega)z = (\mathcal{K}/\omega - \mathrm{J}\omega + j\zeta\mathrm{D})z, \quad \zeta := 1 - \sigma v_o/\omega.$$

where σ is a constant defined in (17). Hence, the ω that maximizes G is given by the minimizer of $\|\mathrm{Q}(j\omega)z\|$. Noting that the matrices J, D, and $\mathcal{K}$ commute, we obtain

$$\|\mathrm{Q}(j\omega)z\|^2 = \|\mathrm{J}z\|^2\omega^2 + \|Kz\|^2/\omega^2 + \zeta^2\|\mathrm{D}z\|^2 - 2z^*\mathcal{K}\mathrm{J}z.$$

Since ζ is fixed by γ as are v_o/ω, the minimum occurs when

$$\|\mathrm{J}z\|^2\omega^2 = \|\mathcal{K}z\|^2/\omega^2,$$

which is satisfied by the ω given in (16).

The γ that maximizes $G(\omega,\gamma)$ in (12) as determined by (18) and (19) can now be found using the ω that maximizes $G(\omega,\gamma)$ as given in (16). During the γ optimization, the resonance frequency ω can be treated as a given constant since it turned out to be independent of γ. The special properties in (20) allow cross terms to cancel such that $\|\hat{u}\|^2$ from (18) can be written as

$$\|\hat{u}\|^2 = \gamma^2\|(\omega^2\mathrm{J}-\mathcal{K})z\|^2 + \gamma^2\|(v_o\Lambda + j\omega\mathrm{D})z\|^2 = \gamma^2\left(q_2v_o^2 - q_1v_o + q_o\right).$$

where

$$q_2 = \|\Lambda z\|^2, \quad q_1 = 2\sigma\omega\|\mathrm{D}z\|^2, \quad q_0 = \|(\omega^2\mathrm{J}-K)z\|^2 + \omega^2\|\mathrm{D}z\|^2.$$

Then, from (12), γ maximizes G when it minimizes

$$\frac{2}{G^2} = \frac{\|\hat{u}\|^2}{v_o^2} = \gamma^2 g_1 + \frac{g_2}{\gamma^2} + g_3,$$

where v_o in (16) is substituted and

$$\begin{aligned}
g_1 &= q_2 - \frac{(z^*\mathrm{C}_o z)q_1}{j\omega z^*\Lambda z} + \frac{(z^*\mathrm{C}_o z)^2 q_o}{(j\omega z^*\Lambda z)^2},\\
g_2 &= \frac{(2e^{\mathsf{T}}C_t e)^2 q_o}{(j\omega z^*\Lambda z)^2},\\
g_3 &= \frac{2(z^*\mathrm{C}_o z)(2e^{\mathsf{T}}C_t e)q_o}{(j\omega z^*\Lambda z)^2} - \frac{(2e^{\mathsf{T}}C_t e)q_1}{j\omega z^*\Lambda z}.
\end{aligned}$$

It can be shown that g_1 and g_2 are positive, and hence $2/G^2$ has a global minimum when

$$\gamma = \sqrt[4]{g_2/g_1}.$$

The expression for γ given in (16) is then obtained by substituting $j\Lambda z = \sigma\mathrm{D}z$. □

The most striking finding in Theorem 4.1 is that the resonance frequency for a natural oscillation, ω, is independent of the environmental drag coefficients and is completely determined by the body mass and stiffness once the mode shape z is fixed. The resonant amplitude of undulation, γ, depends on both body and environmental parameters, where the explicit formula in (16) shows how each factor contributes to its determination. We will gain further insights into the resonant amplitude in the next section.

4.2. Body Resonance vs. Environment Resonance

The previous section showed that the body resonance determines the undulation frequency of the natural gait. This section will show that the environment dynamics are

the dominant factor that determines the resonant amplitude. To this end, first note that the gain in (11) can be factored as

$$G(\omega,\gamma) = \underbrace{\frac{\sqrt{\frac{1}{\mathcal{T}}\int_0^{\mathcal{T}} \|\dot{\phi}(t)\|^2 dt}}{\sqrt{\frac{1}{\mathcal{T}}\int_0^{\mathcal{T}} \|u(t)\|^2 dt}}}_{\mathcal{B}(\omega,\gamma)} \cdot \underbrace{\frac{v_o}{\sqrt{\frac{1}{\mathcal{T}}\int_0^{\mathcal{T}} \|\dot{\phi}(t)\|^2 dt}}}_{\mathcal{E}(\omega,\gamma)}. \tag{21}$$

Each factor has its own meaning. The gain $\mathcal{B}(\omega,\gamma)$ maximizes the body (joint) movement relative to the bending moment needed to generate the joint movement, while the gain $\mathcal{E}(\omega,\gamma)$ maximizes the travel speed with respect to the joint movement required to produce such a speed. Thus the two factors separate the total resonance into those due to body and environment.

Theorem 4.2. *Consider the model in (5), the gait $\phi(t) = \Re[\gamma z e^{j\omega t}]$ with $z = z_{\mathfrak{m}}$ in (9), where $\mathfrak{m}$ is a fixed integer, and the gain G in (11) along with the factors $\mathcal{B}$ and $\mathcal{E}$ in (21). Suppose $\mathtt{c}_n > \mathtt{c}_t$. Then the following statements hold.*

(i) The frequency ω that maximizes the body gain $\mathcal{B}(\omega,\gamma)$ is independent of γ and is given by (16).

(ii) The environmental gain $\mathcal{E}(\omega,\gamma)$ is independent of ω, and the amplitude γ that maximizes $\mathcal{E}$ is given by

$$\gamma = \sqrt{\frac{2n}{\|Tz\|^2} \cdot \frac{c_t}{c_n - c_t}}. \tag{22}$$

Moreover, this amplitude is the lower bound on the γ in (16) that maximizes $G(\omega,\gamma)$, approached in the limit where the stiffness k goes to infinity.

Proof. First note that

$$\sqrt{\frac{1}{\mathcal{T}}\int_0^{\mathcal{T}} \|\dot{\phi}(t)\|^2 dt} = \sqrt{\frac{1}{2}\|j\omega\gamma z\|^2} = \frac{\omega\gamma}{\sqrt{2}}$$

and the velocity v_o is given in (16). Hence $\mathcal{E}$ in (21) is equivalent to

$$\mathcal{E}(\gamma) = \frac{z^*(j\Lambda)z}{(2e^{\mathsf{T}}C_t e)/\gamma + (z^*\mathtt{C}_o z)\gamma}, \tag{23}$$

from which it is clear that $\mathcal{E}$ is independent of ω. Therefore the ω that maximizes $\mathcal{B}$ is the ω that maximizes G in Theorem 4.1, which is given in (16). Moreover, the gain $\mathcal{E}(\gamma)$ is maximized when the denominator takes its minimum, which occurs if the two terms in the denominator are equal. Thus the maximizing γ is given by (22). The statement regarding the lower bound follows by noting that the term $\|(\mathrm{J}\omega^2 - \mathcal{K})z\|$ in (16) is proportional to k. □

It is interesting to note that the amplitude γ in (22) at the environmental resonance is smaller when the directional anisotropy c_n/c_t is larger. This basic property is inherited by γ for the body-environment resonance in (16), with the additional effect of the body flexibility which makes γ larger.

5. Illustrative Example: Leech Swimming

The results in the previous sections are illustrated numerically in the example of the swimming leech, which has been modeled in (J. Chen et al., 2011). Assuming small body deformation, the model can be simplified to (1), which captures the essential dynamics of undulatory swimming, as shown in (Blair & Iwasaki, 2011).

We first show that observed undulatory movements of leeches can be reproduced as the natural gait. The parameter values in the model are set as

$$\ell = 94.8 \text{ mm}, \quad m = 1.16 \text{ g}, \quad k = 58 \text{ mN} \cdot \text{mm/rad},$$
$$c_n = 1.4 \text{ mN/(m/s)}, \quad c_t = 0.12 \text{ mN/(m/s)}, \quad n = 18,$$

where body length ℓ and mass m are those of Leech 1 in (J. Chen et al., 2011), and the body stiffness k and fluid drag coefficients (c_n, c_t) are tuned to roughly match the natural gait swimming with the experimentally observed behavior of Leech 1.

The first mode of the natural gait for the model in (4), as described by Definitions 3.2 and 3.3, are given in Table 1. Experimentally measured values for Leech 1 are also shown for comparison. Here, α denotes the amplitude of oscillation $\max \phi_i$ averaged over the body (over $i = 1 \cdots n-1$); $\alpha := \gamma/\sqrt{n-1}$ for the natural gait. The resonance parameters are calculated numerically using the method in Lemma 3.4 by gridding the (ω, γ) plane. The contour plot in Fig. 3 of the gain G calculated at grid points shows a clear resonance peak.

Table 1. Resonance results for the case study.

	ω (Hz)	α (deg.)	v_o (mm/s)
Natural Gait	2.93	11.3	129
Leech Data (J. Chen et al., 2011)	2.94	11.1	130

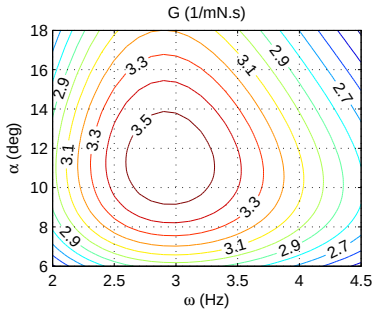

Figure 3. The gain contours showing a resonance peak.

Next we illustrate that, when the natural gait is used for motion planning of robotic systems, the locomotion speed can be adjusted by setting the body stiffness appropriately. The resonant values of ω, α, v_o, and u_{RMS} are calculated for various values of the stiffness k, and plotted as functions of k in Fig. 4. The red and blue curves show the results from (5) and (4), with and without assuming $\theta_o = 0$, respectively. The similarity of the red and blue curves for (ω, α) indicates that the input τ which removes oscillation from the pitch angle θ_o and distinguishes (4) from (5) has little effect on resonance, and the analytical formulas in Theorem 4.1 are accurate. The natural gait at a variety of swim speeds can be generated by adjusting the bending

stiffness k. A slower speed is achieved by decreasing the frequency and increasing the amplitude, while a faster speed is achieved by increasing the frequency with roughly constant amplitude near the lower bound in (22) indicated by the black horizontal line.

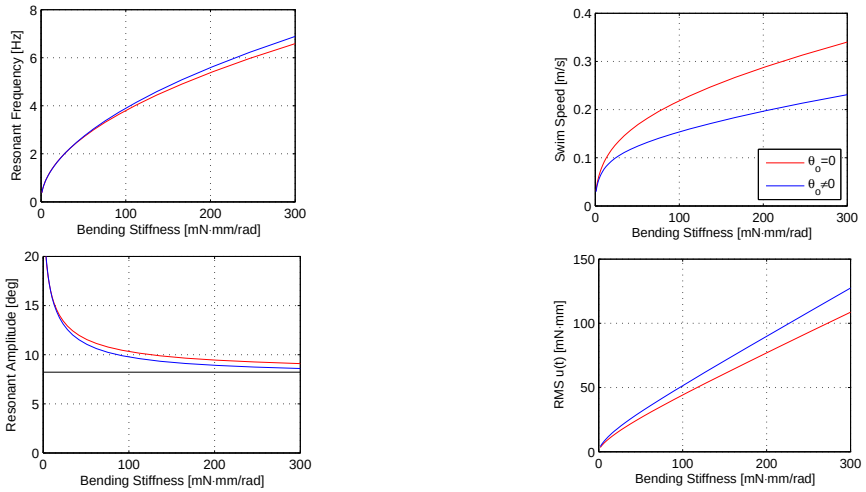

Figure 4. The resonance frequency and amplitude, swim speed, and RMS value of bending moment, as functions of bending stiffness.

We now examine some specific gaits of natural modes 1 and 2 for a body with large/small stiffness. The gait parameter values are calculated for (4) and summarized in Table 2. For each case, 10 snapshots of the body during one cycle of undulation are shown in Fig. 5, where the red and blue bodies indicate the initial and terminal positions. We see that a higher speed is achieved by larger frequency with smaller amplitude (or curvature) within the same mode. The snapshots indicate that the body pushes water behind to generate thrust, with a larger slide at a higher speed. The slip is very small at a low speed so that the tail almost follows the trajectory of the head. Comparing (a) and (c), the second mode of the natural gait achieves (roughly) the same speed as the first mode by a higher frequency with a smaller bending moment. The leeches normally use the first mode, showing their preference of a low frequency over a low muscle tension. The second mode may be useful for robotic applications when the locomotion has to occur in a narrow channel.

Table 2. Natural gaits at two modes with large/small stiffness

	$\mathfrak{m}$	k	ω	α	v_o	u_{RMS}
Case	mode	$\frac{\text{mN·mm}}{\text{rad}}$	Hz	deg	mm/s	mN·mm
(a)	1	300	6.89	8.59	231	128
(b)	1	5	0.85	18.6	58.4	7.00
(c)	2	60	11.0	16.6	237	46.9
(d)	2	0.5	1.00	31.7	34.9	1.12

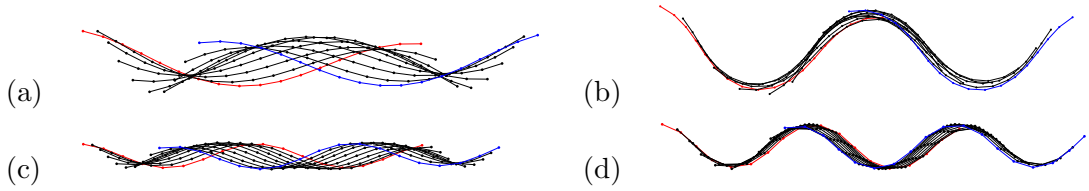

Figure 5. Snapshots of the natural gaits over one cycle for cases (a)–(d) in Table 2 on the same scale (swimming to right).

6. Conclusion

We have shown that the origin of traveling waves observed in undulatory locomotion can be traced to natural oscillations of idealized dynamics as detailed in Theorem 3.1. For this system, the natural mode shape z, specified in Definition 3.2, is shown to have a constant magnitude and linearly changing phase along the body. The total phase lag from head to tail for the $\mathfrak{m}^{\text{th}}$ mode approaches $2\mathfrak{m}\pi$ as the number of links n increases, which gives $\mathfrak{m}$ waves exhibited by the body at each time instant. For each mode, the gain from the bending moment to the locomotion speed is shown to have a peak that defines the resonant frequency and amplitude (ω, γ) for which explicit formulas are derived in Theorem 4.1.

The resonant frequency ω given in Theorem 4.1 depends only on the body stiffness and body inertia and is clearly analogous to the undamped natural frequency of a standard mechanical system. This ω not only maximizes the gain G used in Definition 3.3, but also the gain $\mathcal{B}$ in (21) which goes from the bending moment to the joint movement. The input-output system for which the gain $\mathcal{B}$ is defined is linear, so it is not surprising that resonance is independent of amplitude. However, the input-output system for which the gain G is defined is nonlinear with resonance occurring at a particular amplitude, so it is consequential that the resonant frequency is independent of the amplitude and equivalent to the frequency maximizing $\mathcal{B}$.

The resonant amplitude γ given in Theorem 4.1 depends on both the body properties and the drag coefficients. It is not independent of ω. However the γ that maximizes the gain $\mathcal{E}$ from the joint movement to the travel velocity is independent of ω and depends only on the drag coefficients. When the difference between the normal and tangential drag coefficients becomes smaller, γ increases to compensate. This is intuitive since larger body waves increase normal drag with no effect on tangential drag, thereby increasing thrust.

In conclusion, Definitions 3.2 and 3.3 fully describe an undulatory gait for a long, slender body subject to resistive anisotropic forces from the environment. The natural gait can be calculated in an instant using the explicit formulas that analytically show how the gait is affected by system parameters. The gait exploits natural dynamics of the body-environment system for efficient locomotion, and the travel speed can be adjusted by setting the resonance appropriately through the stiffness value. The result is useful for designing gaits of robotic locomotors as well as for understanding the mechanisms underlying undulatory locomotion observed in nature.

Acknowledgment

This work was supported by NSF grant no. 1335545.

References

Ahlborn, B. K., Blake, R. W., & Megill, W. M. (2006). Frequency tuning in animal locomotion. *Zoology*, *109*, 43-53.

Blair, J., & Iwasaki, T. (2011). Optimal gaits for mechanical rectifier systems. *IEEE Trans. Auto. Contr.*, *56*(1), 59-71.

Borazjani, I., & Sotiropoulos, F. (2008). Numerical investigation of the hydrodynamics of carangiform swimming in the transitional and inertial flow regimes. *J. Exp. Biol.*, *211*, 1541-1558.

Borazjani, I., & Sotiropoulos, F. (2009). Numerical investigation of the hydrodynamics of anguilliform swimming in the transitional and inertial flow regimes. *J. Exp. Biol.*, *212*, 576-592.

Chen, J., Friesen, W. O., & Iwasaki, T. (2011). Mechanisms underlying rhythmic locomotion: Body-fluid interaction in undulatory swimming. *J. Exp. Biol.*, *214*(4), 561-574.

Chen, Z., Iwasaki, T., & Zhu, L. (2015). Feedback control for natural oscillations of locomotion systems under continuous interactions with environment. *IEEE Trans. Contr. Sys. Tech.*, *23*, 1294-1306.

Collins, S., Ruina, A., Tedrake, R., & Wissei, M. (2005). Efficient bipedal robots based on passive-dynamic walkers. *Science*, *307*, 1082-1085.

Cortes, J., Martinez, S., Ostrowski, J. P., & McIsaac, K. A. (2001). Optimal gaits for dynamic robotic locomotion. *Int. J. Robot. Res.*, *20*(9), 707-728.

Curet, O., Patankar, N., Lauder, G., & MacIver, M. (2011). Mechanical properties of bio-inspired robotic knifefish with an undulatory proopulsor. *Bioinspiration & Biomimetics*, *6*(2), 026004.

Fukuoka, Y., Kimura, H., & Cohen, A. (2003). Adaptive dynamic walking of a quadruped robot on irregular terrain based on biological concepts. *Int. J. Robotics Research*, *22*(3-4), 187-202.

Gazzola, M., Argentina, M., & Mahadevan, L. (2015). Gait and speed selection in slender inertial swimmers. *Proc. Nat. Aca. Sci.*, *112*(13), 3874-3879.

Grizzle, J., Abba, G., & Plestan, F. (2001). Asymptotically stable walking for biped robots: analysis via systems with impulse effects. *IEEE Trans. Auto. Contr.*, *46*(1), 51-64.

Hatton, R. L., & Choset, H. (2010). Generating gaits for snake robots: Annealed chain fitting and keyframe wave extraction. *Auton Robot*, *28*, 271-281.

Hicks, G., & Ito, K. (2005). A method for determination of optimal gaits with application to a snake-like serial-link structure. *IEEE Trans. Autom. Control.*, *50*(9), 1291-1306.

Hirose, S. (1993). *Biologically inspired robots: Snake-like locomotors and manipulators*. Oxford University Press.

Holt, K., Hamill, J., & Anders, R. (1991). Predicting the minimal energy cost of human walking. *Med. and Sci. in Sports and Exercise*, *23*, 491-498.

Ijspeert, A. J. (2008). Central pattern generators for locomotion control in animals and robots: A review. *Neural Networks*, *21*(4), 642-653.

Ijspeert, A. J. (2014). Biorobotics: Using robots to emulate and investigate agile locomotion. *Science*, *346*, 196-203.

Ijspeert, A. J., Crespi, A., Ryczko, D., & Cabelguen, J. M. (2007). From swimming to walking with a salamander robot driven by a spinal cord model. *Science*, *315*(5817), 1416-1420.

Kohannim, S., & Iwasaki, T. (2014). Analytical insights into optimality and resonance in fish swimming. *J. R. Soc. Interface*, *11*(20131073).

Kohannim, S., & Iwasaki, T. (2017). Dynamical model and optimal turning gait for mechanical rectifier system. *IEEE Trans. Auto. Contr.*, *62*(2), 682-693.

Leftwich, M. C., Tytell, E. D., Cohen, A. H., & Smits, A. J. (2012). Wake structures behind a swimming robotic lamprey with a passively flexible tail. *J. Exp. Biol.*, *215*, 416-425.

Lewin, G., & Haj-Hariri, H. (2003). Modelling thrust generation of a two-dimensional heaving airfoil in a viscous flow. *J. Fluid. Mech.*, *492*, 339-362.

Lighthill, M. (1969). Hydrodynamics of aquatic animal propulsion. *Ann. Rev. Fluid. Mech.*,

1, 413-446.
Liu, X., Fish, F., Russo, R., Blemker, S., & Iwasaki, T. (2016). Modeling and optimality analysis of pectoral fin locomotion. *Chapter 11, Neuromechanical Modeling of Posture and Locomotion, Eds. B. Prilutsky and D.H. Edwards, Springer Series in Computational Neuroscience*, 309-332.
Long, J. H., & Jr. (1998). Muscles, elastic energy, and the dynamics of body stiffness in swimming eels. *Amer. Zool.*, *38*, 771-792.
Ludeke, T., & Iwasaki, T. (2017). Natural modes and resonance in undulatory locomotion. *IEEE Am. Cont. Conf. Proc.*, 5443-5448.
McGeer, T. (1990). Passive dynamic walking. *Int. J. Robotics Research*, *9*(2), 62-82.
McIsaac, K. A., & Ostrowski, J. P. (2003). Motion planning for anguilliform locomotion. *IEEE Trans. Robot. Autom.*, *19*(4), 637-652.
Moored, K., Dewey, P., Smits, A., & Haj-Hariri, H. (2012). Hydrodynamic wake resonance as an underlying principle of efficient unsteady propulsion. *J. Fluid Mech.*, *708*, 329-348.
Saito, M., Fukaya, M., & Iwasaki, T. (2002). Serpentine locomotion with robotic snake. *IEEE Control Systems Magazine*, *22*(1), 64-81.
Sitti, M., Menciassi, A., Ijspeert, A. J., Low, K. H., & Kim, S. (2013). Survey and introduction to the focused section on bio-inspired mechatronics. *IEEE Trans. Mechatronics*, *18*(2), 409-418.
Tesch, M., Lipkin, K., Brown, I., Hatton, R., Peck, A., Rembisz, J., & Choset, H. (2009). Parameterized and scripted gaits for modular snake robots. *Adv. Robotics*, *23*, 1131-1158.
Triantafyllou, M., Triantafyllou, G., & Yue, D. (2000). Hydrodynamics of fishlike swimming. *Annu. Rev. Fluid Mech.*, *32*, 33-53.
Wagenaar, R., & van Emmerik, R. (2000). Resonant frequencies of arms and legs identify different walking patterns. *J. of Biomechanics*, *33*, 853-861.

Appendix A. Terms in the Equation of Motion

The coefficient matrices in (1) are defined by

$$\begin{aligned}
&J := LML/3 + F^\mathsf{T} MF, \quad D := D_\tau + D_n, \\
&D_\tau := LC_nL/3, \quad D_n := F^\mathsf{T} C_n F, \quad \Lambda := \Lambda_n - \Lambda_t, \\
&\Lambda_t := F^\mathsf{T} C_t - \mathrm{diag}(F^\mathsf{T} C_t e), \quad \Lambda_n := F^\mathsf{T} C_n, \\
&F := M^{-1}B(B^\mathsf{T} M^{-1} B)^{-1} AL, \\
&C_o := C_n - C_t, \quad K := B\mathcal{K}B^\mathsf{T}, \quad e := \begin{bmatrix} 1 & \cdots & 1 \end{bmatrix}^\mathsf{T}, \\
&A := \begin{bmatrix} I & o \end{bmatrix} + \begin{bmatrix} o & I \end{bmatrix}, \quad B^\mathsf{T} := \begin{bmatrix} I & o \end{bmatrix} - \begin{bmatrix} o & I \end{bmatrix},
\end{aligned} \tag{A1}$$

where o is the $n-1$ dimensional zero vector, M, L, C_n, and C_t are $n \times n$ diagonal matrices with mass, half length, normal drag coefficient, and tangential drag coefficient for each link on the diagonal, and $\mathcal{K}$ is a $(n-1) \times (n-1)$ diagonal matrix of joint stiffness coefficients.

When the mass and normal drag coefficient are proportional to each other for each link, the moment of inertia and environmental drag matrices are proportional as well:

$$C_n = \eta M \quad \Rightarrow \quad D = \eta J,$$

where $\eta \in \mathbb{R}$ is a proportionality constant. This is the case under the uniform link assumption (2) with $\eta = c_n/m_o$.

The coefficient matrices in (5) and (15) are defined by

$$\begin{aligned}
&\begin{bmatrix} J_{11} & J_{12} \\ J_{21} & J_{22} \end{bmatrix} := \begin{bmatrix} T^{\mathsf{T}} \\ e^{\mathsf{T}} \end{bmatrix} J \begin{bmatrix} T & e \end{bmatrix}, && T := B(B^{\mathsf{T}}B)^{-1}, \\
&\mathsf{J} := J_{11}, && \mathsf{D} := D_{11}, && \mathsf{\Lambda} := \Lambda_{11}, \\
&\mathcal{J} := \mathsf{J} - hJ_{21}, && \mathcal{D} := \eta\mathcal{J}, && \mathcal{L} := \mathsf{\Lambda} - h\Lambda_{21},
\end{aligned} \qquad h := J_{12}J_{22}^{-1}, \tag{A2}$$

and Λ_{ij} and D_{ij} with $i, j = 1, 2$ are defined for Λ and D by the same congruence transformation as in J_{ij}. Note that Λ_{12} and Λ_{22} are zero under (2).